Dipole Configurations with Strongly Improved Radiation Efficiency for Hand-Held Transceivers

Roger Yew-Siow Tay, *Member, IEEE*, Quirino Balzano, *Senior Member, IEEE*, and Niels Kuster, *Member, IEEE*

***Abstract*— In this paper the design criteria for antenna structures with improved radiation efficiency while operating in close vicinity to a biological scatterer were investigated. The study was performed using a simple $\lambda/2$ dipole combined with a directive or reflective element. The optimization criteria were the effective radiation efficiency, the spatial peak specific absorption rate (SAR), and the sensitivity of the input resistance to the distance from the scatterer. It could be demonstrated that the primary design criterion to improve the radiation efficiency is not directivity but the reduction of the maximum incident magnetic field strength in the exposed skin area of the user's head. For the reflectively coupled dipole, all performance parameters could be improved by several decibels compared to a standard $\lambda/2$ dipole, whereas for some other directive structures, the performance was impaired. The study was conducted with the generalized multipole technique (GMT) numerical simulation method, the results of which were validated by measurement methods.**

***Index Terms*— Design criteria, directional antennas, mobile phones, radiation efficiency, SAR.**

I. Introduction

SINCE the introduction of cellular phone service, industry has succeeded in greatly reducing the size and weight of hand-held mobile telecommunications equipment (MTE). Performance has been greatly improved and functionality has been greatly expanded, but with few exceptions, antenna configurations have remained basically the same. Most currently employed antennas are helical antennas and monopole antennas, some of them with reduced length. In general, short antennas and reduced separation between the antenna and the head increase energy loss into the head of the user [1]. If the device is not carefully designed, a considerable amount of the power available at the feed point of the antenna may be absorbed in the user's head [2]–[4]. Comparisons of current commercial devices show that the performance with respect to user exposure varies greatly between the different designs. In general, large absorption values correlate with poor radiation performance [5], [6].

Therefore, significant power loss in the head is not only an issue of achieving compliance with safety limits [5] since excellent radiation efficiency provides distinguished technical advantages such as longer talk time or smaller and lighter batteries. A major constraint regarding the design of highly efficient devices, however, is the consumer's desire for compact design of both antenna and device.

An obvious design approach, which satisfies the requirement for compactness and limited exposure, is the use of a planar antenna integrated onto the back side (away from the head) of the hand-held MTE. The effectiveness of such an antenna design was investigated [7]. Although the study showed significant reduction of the absorption in the user's head, this approach brings additional design restrictions and difficulties. For example, effective design measures must be found to prevent the user from covering the antenna with his/her hand or while shouldering the phone. Another difficulty is in achieving the required bandwidth and efficiency for a small device. Nevertheless, cellular phones with planar antennas have lately become commercially available.

Directivity can also be achieved through other antenna concepts, e.g., dipole structures combined with directors and/or reflectors. The advantages and disadvantages of directional antennas were discussed in [8] on the basis of a study performed with an array structure of four small dipoles in the vicinity of a lossy sphere. The various approaches described in the literature were also discussed. One of the general conclusions of this paper was that power absorption into the head of the operator is effectively reduced by increased antenna directivity.

Contracting this general statement, which is based on a radiation model, the study on the absorption mechanism in biological bodies in the near field of dipole antennas [1] would suggest that increased directivity does not necessarily result in improved efficiency. The reason is that the energy absorbed in the head is proportional to the square of the magnetic field strength at the location of the tissue [1], i.e., the energy absorption mechanism is predominantly an induction and not a radiation phenomena. Therefore, the design goal for antennas of improved efficiency would not be primarily to attain enhanced directivity, but to minimize the H-field incident on the user's face.

The objective of this paper is to verify this design goal on a $\lambda/2$ dipole antenna combined with a director or a reflector for operation in the close vicinity of a very lossy scatterer. In addition, the suitability of such structures for hand-held transmitters is evaluated.

II. Parameters of Optimization

Today, not only do technical considerations govern the design of antennas for hand-held MTE, but economics and aesthetics also play critical design roles. In this paper, only

Manuscript received April 1, 1997; revised February 6, 1998.

R. Y.-S. Tay and Q. Balzano are with the Motorola Corporate Electromagnetics Research Laboratory, Plantation, FL 33322 USA.

N. Kuster is with the Swiss Federal Institute of Technology (ETH), Zurich, CH-8092 Switzerland.

Publisher Item Identifier S 0018-926X(98)05032-7.

radiation efficiency, the specific absorption rate, and input impedance stability have been employed as criteria for optimization.

A. Effective Radiation Efficiency

The effective radiated power $P_{r'}$ is the power available for communication, i.e., the power which is actually radiated away from the user. It can be determined by integrating the normal component of the time-averaged Poynting vector $P_{\rm av}$ over a closed surface $\boldsymbol{S}$, which encloses the antenna and the user

$$P_{r'} = \oint_{\partial V} P_{\rm av}\, d\boldsymbol{S} = \oint_{\partial V} \tfrac{1}{2}\,\mathrm{Re}\{\boldsymbol{E}\times\boldsymbol{H}^*\}\cdot d\boldsymbol{S} \qquad (1)$$

where $\boldsymbol{E}$ and $\boldsymbol{H}$ are the electric and magnetic field vectors (amplitudes).

The effective radiated efficiency η is, therefore, the ratio between the power available for communications $P_{r'}$ and the antenna input power $P_{\rm in}$

$$\eta = \frac{P_{r'}}{P_{\rm in}} = \frac{P_{r'}}{P_{r'} + P_{\rm abs} + P_{\rm diss}}. \qquad (2)$$

$P_{\rm diss}$ is the RF power dissipated in the lossy dielectric material of the antenna and enclosure. The power absorbed in the user $P_{\rm abs}$ can be found either by the surface integral of the normal component of the time-averaged Poynting vector $P_{\rm av}$ entering the surface $S_{\rm scat}$ of the lossy scatterer or by integrating the specific absorption rate (SAR) over the entire volume of the scatterer (user)

$$P_{\rm abs} = \oint_{S_{\rm scat}} P_{\rm av}\, d\boldsymbol{S}_{\rm scat} = \int_{V_{\rm scat}} \varrho\,\mathrm{SAR}\, dV_{\rm scat} \qquad (3)$$

where ϱ is the density of the tissue and SAR is defined below.

B. Specific Absorption Rate (SAR)

SAR is the incremental electromagnetic power absorbed by an incremental mass contained in a volume element of given density and is expressed by

$$\mathrm{SAR} = \frac{\sigma}{\varrho}(E_x^2 + E_y^2 + E_z^2) \qquad (4)$$

where σ is the equivalent conductivity ($\sigma = \omega\epsilon''$) and ϱ the mass density of the tissue. E_x, E_y, E_z are the orthogonal root mean square (rms) components of the E-field in the tissue.

C. Input Resistance Stability

To achieve high efficiency, the driving-point impedance and output impedance of the transmitting circuit should be closely matched. However, the input impedance of antenna systems operating in close vicinity of scattering objects such as a user's head may significantly depend on the proximity to the head. Small variations of the driving point impedance due to variation of the distance between the head and the antenna would be greatly desirable. The rate at which the input resistance changes is defined as

$$\zeta = \frac{\mathrm{Re}\{Z_{fs}\} - \mathrm{Re}\{Z_{\rm load}\}}{\mathrm{Re}\{Z_{fs}\}} \qquad (5)$$

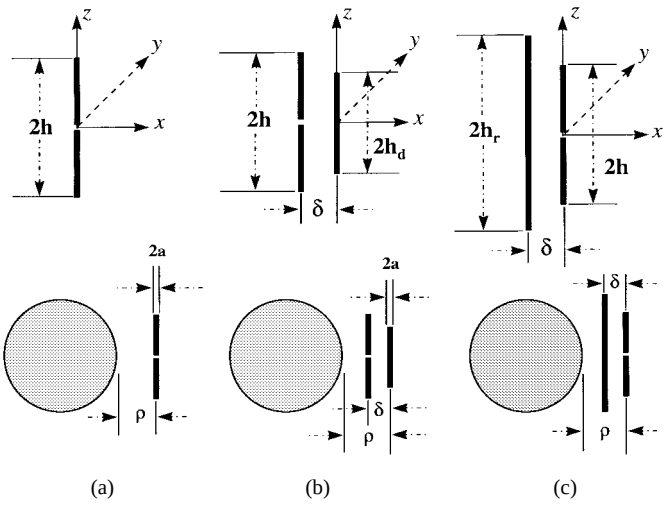

Fig. 1. Length and spacing definitions of the studied antenna structures in free-space (top) and in the proximity of the spherical scatterer (bottom). (a) Center-fed $\lambda/2$ dipole. (b) Center-fed $\lambda/2$ dipole coupled to a directive element. (c) Center-fed $\lambda/2$ dipole coupled to a reflective element.

where $\mathrm{Re}\{Z_{fs}\}$ and $\mathrm{Re}\{Z_{\rm load}\}$ are the real parts of the driving-point impedance for the antenna in free-space and in the presence of the spherical phantom, respectively.

III. Antenna Configuration

The performance of real MTE, when used on the street, depends on a wide range of parameters, as has been described in [2]. These include:

- operational frequency and antenna input power;
- entire mechanical and RF design of the device including mounting location of the antenna, antenna type and configuration, feeding network, etc.;
- position of the device with respect to the head;
- outer shape of the head;
- distribution of the different tissues within the head;
- electrical properties of these tissues.

In order to evaluate the performance and potential effectiveness of a dipole structure combined with parasitic elements, it was necessary to reduce this large parameter space to a simple configuration in order to derive the fundamental interaction properties. To reduce computational requirements and improve the reliability of the numerical results, the symmetrical configurations shown in Fig. 1 were utilized.

The antenna configurations used in this analysis are fully described in Fig. 1. The length of the active element $2\boldsymbol{h}$ was $\lambda/2$ in all evaluated configurations, i.e., 160 mm at 900 MHz. The radii of the active and the parasitic elements are 1 mm. The antenna diameter was not varied in this study, since the dependence of the performance on the radius of the wire is very small for thin wires. Various parameters were varied in the course of this study, the results of which were compared to those of the simple $\lambda/2$ dipole. The varied parameters were as follows:

- the separation δ between the active $\lambda/2$ dipole and the parasitic element from 5 to 50 mm in steps of 5 mm;

- the length of the parasitic element $2\boldsymbol{h}_p$ or the ratio $\boldsymbol{k}$ of the length of the parasitic to those of the active elements ($\boldsymbol{k} = \boldsymbol{h}_p/\boldsymbol{h}$) from 0.125 to 2.0:
  $\boldsymbol{h}_p \equiv \boldsymbol{h}_d$—parasitic element acts as director;
  $\boldsymbol{h}_p \equiv \boldsymbol{h}_r$—parasitic element acts as reflector;
- the separation ρ between the surface of the spherical head phantom and the center of the antenna element from 5 to 50 mm in steps of 5 mm.

The modeling of the head was reduced to a sphere of diameter 200 mm having the dielectric parameters of $\epsilon_r = 43.5$ and $\sigma = 0.85\mho$/m, which correspond to those of brain tissue at 900 MHz. The density was taken to be $\varrho = 1000\ \mathrm{kg/m^3}$, which is slightly below the density of brain tissue ($\approx 3\%$) but simplifies the comparison with results given elsewhere in $\mathrm{mW/cm^3}$. This phantom is identical to the spherical phantom used in [2], which resulted in RF absorption characteristics that tally well with those of the anatomically correct head phantom based on high-resolution magnetic resonance imaging (MRI) scans of different adults and children [2]–[4], [9].

IV. Simulation Technique

The three-dimensional (3-D) multiple multipole (MMP-3-D) code, which is based on the generalized multipole technique (GMT), was the numerical method chosen for this study. This technique has proven to be suitable for the detailed and accurate evaluation of symmetrical antennas [10] and has proven to have several conceptual advantages for antennas operating in the close vicinity of simple scatterers [4], [11]. Details about GMT and the MMP-3-D code are given in [12].

V. Experimental Setup and Techniques

A. Setup

Experimental techniques were employed to verify qualitatively the findings obtained through simulations. A quantitative verification was not striven for since this study was not designed to validate the numerical approach but to study and verify basic design criteria. The experimental antenna prototype for the frequency of 900 MHz was built, as shown in Fig. 2. It consists of a balanced center-fed $\lambda/2$ dipole and a Teflon™ fixture holding the parasitic elements. The separation of the parasitic elements from the dipole can be simply adjusted and the two parasitic arms are also easily exchanged. Since the driving impedance drops with decreased spacing between the dipole and parasitic element, the impedance was matched with a "*three top tuner*" (Maury Microwave Corporation, CA, Model 1878A S/N 846). The forward and reflected power were monitored with a bi-directional coupler.

Previous studies have shown [2], [3], [9] that the curvature of the phantom does not strongly alter the absorption distribution nor the spatial peak SAR. Therefore, the quite laborious fabrication of a spherical phantom could be omitted and an available human head–torso phantom [13] was used instead. Nevertheless, to achieve the closest possible correspondence between numerical and experimental modeling, the antenna was positioned at the upper back of the head, the location at which the phantom has a curvature similar to that of the numerical model. The phantom was filled with a sugar-salt-water solution produced according to the recipe [14]. The dielectric parameters measured by the slotted line technique were $\epsilon_r = 44$ and $\sigma = 1.0\mho$/m.

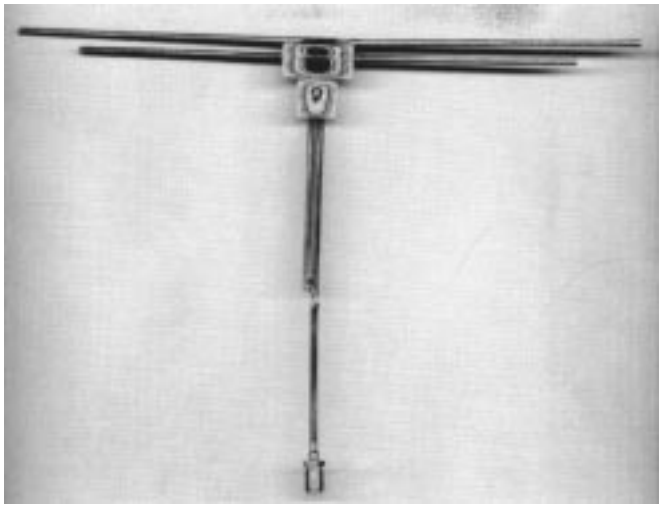

Fig. 2. Experimental antenna prototype.

B. Applied Techniques

The near-field measurements were conducted using miniature $\boldsymbol{E}$- and $\boldsymbol{H}$-field probes positioned with a robotic scanner (DASY2). A detailed description of the system is given in [15]. This automated system provides accurate quantitative assessments with high spatial resolution [16].

VI. Results in Free-Space

According to [1], the directivity of an antenna does not necessarily result in reduced absorption and improved efficiency since the fields are predominately induced in the tissue by the H-field. The capacitive coupling is of minor importance compared to the inductive coupling because of the high permittivity of living tissue. Hence, the square of the magnetic field strength at the location of the surface of the human head is a reliable qualitative indication of the expected losses [1] and should be the subject of minimization.

To test this prediction, the H-field generated in the close vicinity of the antenna is first analyzed in free-space. Then the effective radiation efficiency, the spatial peak SAR as well as the sensitivity on the driving-point resistance are determined in the vicinity of the spherical scatterer.

Figs. 3–5 show (1) the analysis of the amplitude ratio and the phase difference of the current in the parasitic element to the active ($\lambda/2$ dipole) element, (2) the directivity in the xy plane (azimuth cut), and (3) the radiation resistance as a function of the element length ratio $\boldsymbol{k}$ and the separation δ. The real part of the driving-point impedance was equivalent to the radiation resistance since the conductive structures were simulated as perfectly conductive elements. These figures illustrate the coupling mechanisms of the parasitic elements as a function of the separation between active ($\lambda/2$ dipole) and

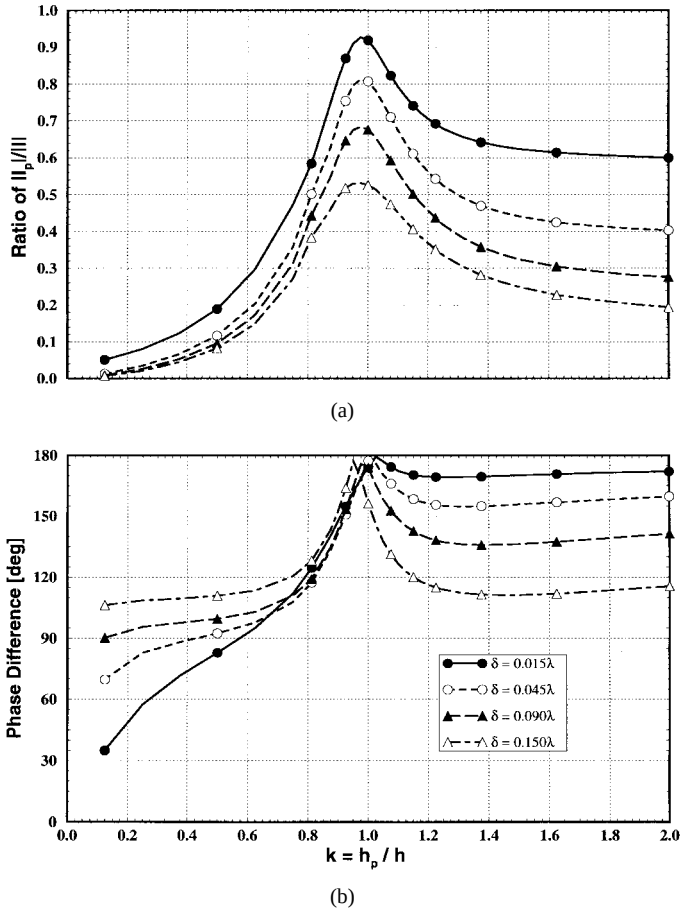

Fig. 3. (a) Comparison between the ratio of the current amplitude and (b) the phase difference in the parasitic element to the current in the active ($\lambda/2$ dipole) element versus $\boldsymbol{k}$. The separation δ between radiator and parasitic element is varied from 0.015λ to 0.15λ. The simulations were performed at 900 MHz.

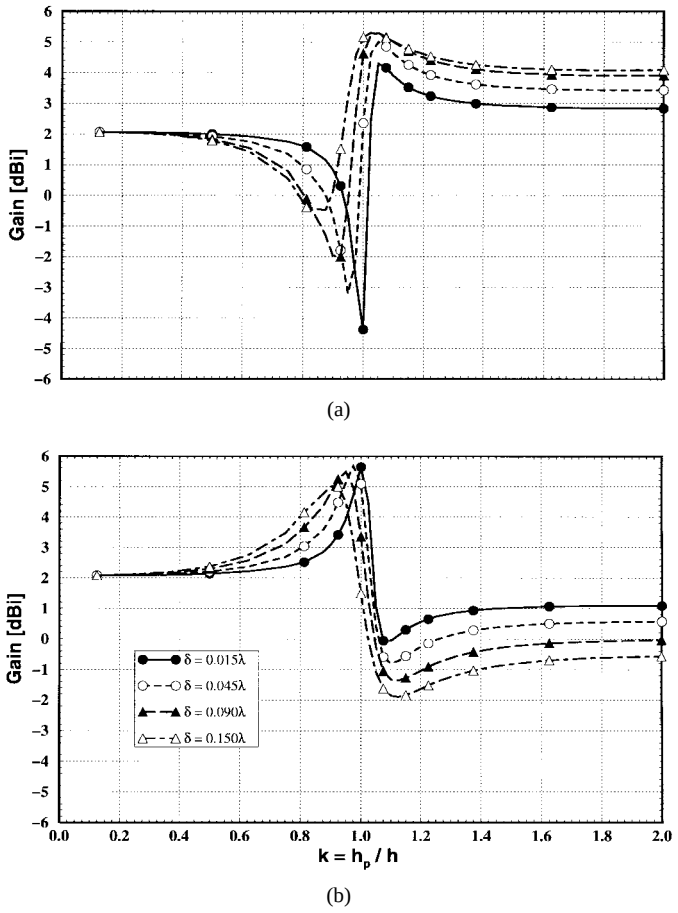

Fig. 4. Plot of the directivity of the parasitically coupled dipole in (a) the direction of $(-x)$ and (b) $(+x)$ versus $\boldsymbol{k}$ in free-space. The separation δ between radiator and parasitic element is varied from 0.015λ to 0.15λ (i.e., 5 mm to 50 mm at 900 MHz).

parasitic element. The results were compared to a $\lambda/2$ dipole and they can be summarized as follows.

- For $\boldsymbol{k} < 0.5$, the coupling of electromagnetic energy between the active ($\lambda/2$ dipole) and the parasitic elements is very low. Hence, the change in the radiation performance is also small (Figs. 4 and 5).
- For $\boldsymbol{k} \approx 1$, the coupling of electromagnetic energy between the active ($\lambda/2$ dipole) and the parasitic elements is large; the current induced on the parasitic element is maximized and is 180° out of phase from the active $\lambda/2$ dipole element. Hence, the radiation efficiency is minimized for constant current excitation (Figs. 3 and 5).
- For $\boldsymbol{k} > 1.2$, the incremental radiation performance enhancement is minimal as $\boldsymbol{k}$ increases (Figs. 4 and 5).

An important constraint for mobile phones is the dimensions of the antenna structure (separation δ and height) because of aesthetic and ergonomic considerations. A low input impedance is equivalent to large currents on the antenna elements, which generate large H-field strengths in their vicinity. To investigate whether the cancellation of the different H-field components due to the phase shift can become sufficient in the vicinity of the antenna structure to provide a lower total magnetic field strength than the single dipole, the magnitude of

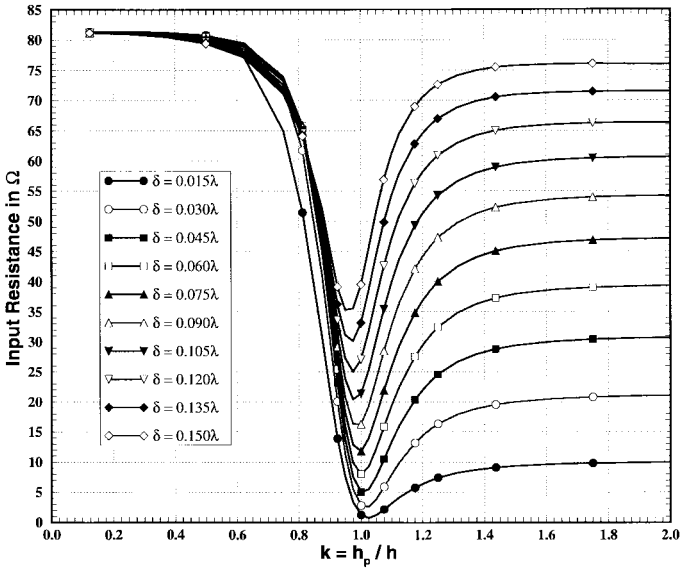

Fig. 5. Plot of the radiation resistance in free-space versus $\boldsymbol{k}$. The separation δ between radiator and parasitic element is varied from 0.015λ to 0.15λ (i.e., 5 mm to 50 mm at 900 MHz).

the magnetic field was plotted at $x = 15$ mm as a function of the ratio $\boldsymbol{k}$ (Fig. 6). Concluding from this plot, the magnetic field at the side of the potential user is only reduced if the

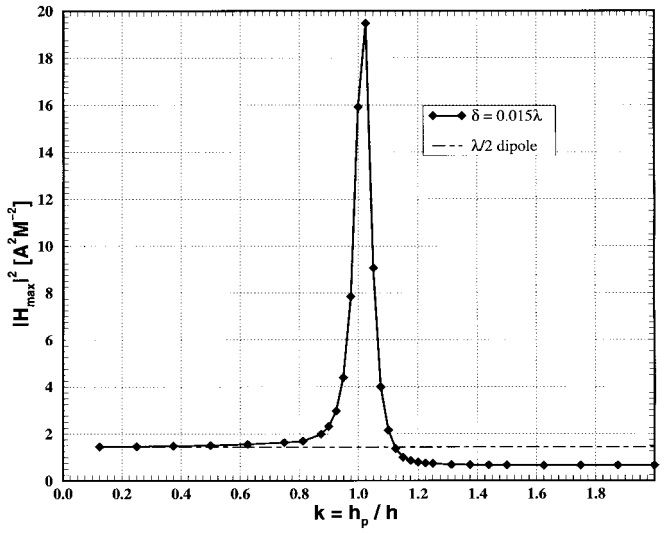

Fig. 6. Plot of the maximum H-field at $x = -15$ mm in free-space versus $\boldsymbol{k}$. The separation distance δ between active ($\lambda/2$ dipole) and parasitic elements is 0.015λ. The simulations were performed at 900 MHz and the radiated power was normalized to 1 W.

parasitic element is placed between the user and the active ($\lambda/2$ dipole) element, and if $\boldsymbol{k}$ is greater than 1.125. The other configurations would not reduce the H-field at this location and, if the prediction derived from [1] is correct, would not result in lower exposure nor increase radiation efficiency, although they would provide directivity.

The separation constraint between antenna and face is the maximum distance at which an antenna element can be placed, i.e., the separation ρ. In the real world, this maximum separation is equivalent to the thickness of the device. Even considering this constraint, the H-field strength for the reflectively coupled dipole is substantially lower than for the $\lambda/2$ dipole, as is shown in Fig. 7 for $x = -15$ mm (corresponds to $\rho = 15$ mm). The directively coupled dipole, having a similar directivity, generates significantly increased magnetic field strengths due to the closer proximity of the active dipole.

The advantages of the reflectively coupled dipole diminish for small distances ($\rho < 12$ mm), as shown in Fig. 8, because of the large magnetic field in the immediate vicinity of the parasitic element due to the low driving-point impedance of the dipole. In hand-held MTE applications, the antenna would have to be designed so that the user's face does not coincide with this region. From this standpoint, the configuration with $\boldsymbol{k} = 1.0625$, which generates strongly enhanced H-field values for distances up to 20 mm, would not be applicable.

The measured and computed distribution of the H-field strength is shown in Figs. 9 and 10 for the plane $x = -10$ mm. The measured and simulated E-field in the same evaluation plane also agreed well, which gave us sufficient confidence in the free-space result.

VII. Results with Scatterer

Whether the observed rather large reduction of the H-field in the case of the reflectively coupled dipole still translates to improved performance in close vicinity to the lossy scatterer is

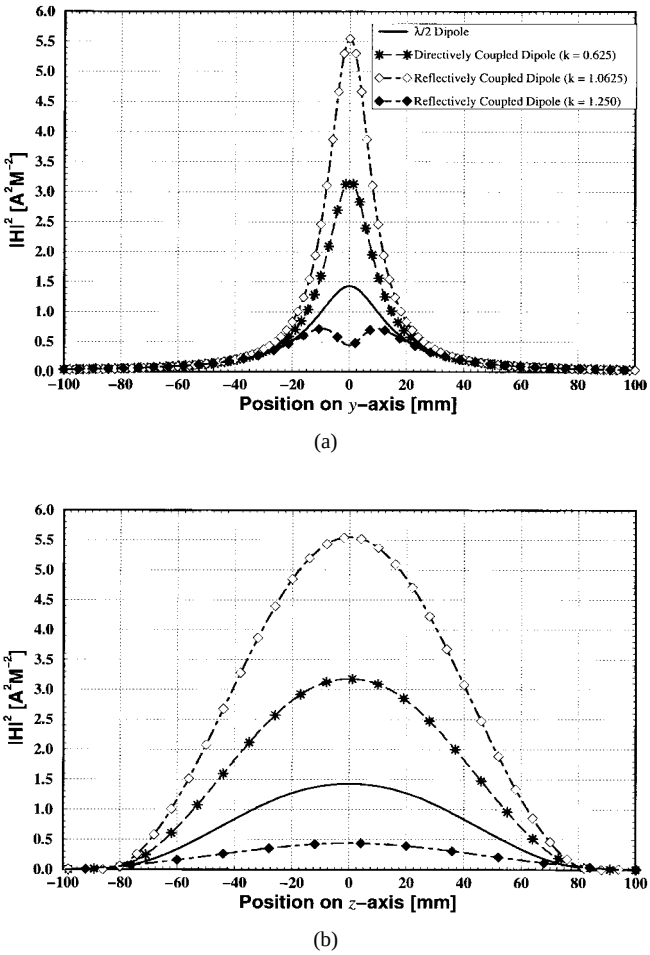

Fig. 7. (a) Plot of $|\boldsymbol{H}|^2$ on the z axis (at $x = -15$ mm, $y = 0$) and (b) y axis (at $x = -15$ mm, $z = 0$) for four selected configurations. The separation between the $\lambda/2$ dipole and the parasitic element is $\delta = 0.015\lambda$. The simulations were performed at 900 MHz with the radiated power normalized to 1 W.

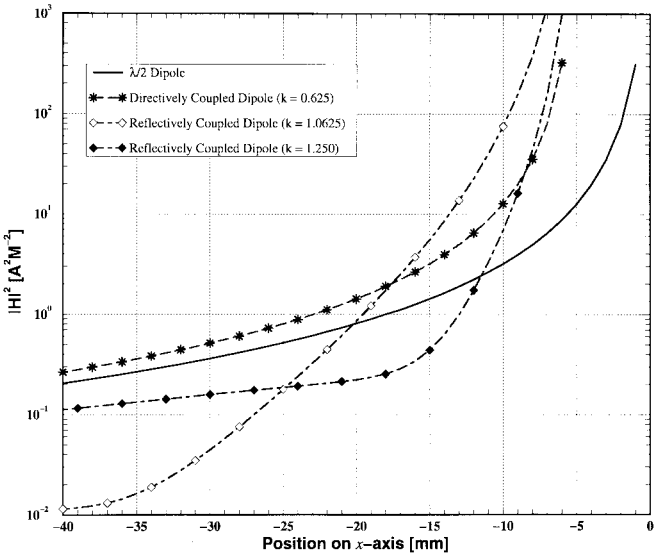

Fig. 8. Plot of the peak $|\boldsymbol{H}|^2$ in the plane $z = 0$ as a function of x. Compared are the peak values in free-space for the same configurations, as shown in the previous figure.

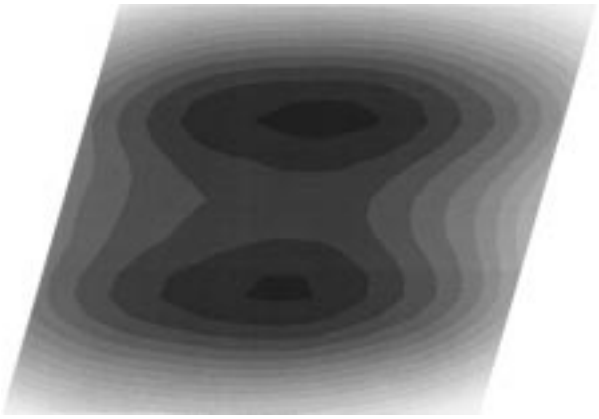

Fig. 9. Measured H-field distribution of the reflectively coupled dipole ($\boldsymbol{k} = 1.25; \delta = 5$ mm, $f = 900$ MHz) in the plane $x = -10$ mm. The input power was 0.985 W. The darker central shading denotes a higher H-field intensity, which moves to a lighter (lower H-field intensity) shading at the outer edges.

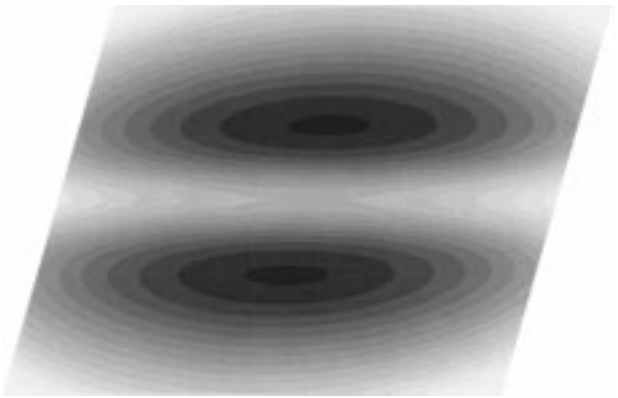

Fig. 10. Simulated H-field distribution of the reflectively coupled dipole ($\boldsymbol{k} = 1.25, \delta = 5$ mm, $f = 900$ MHz) in the plane $x = -10$ mm. The radiated power was normalized to 1 W and plotted in the same fashion as the previous figure.

the subject of this section. Endpoints to be investigated were effective radiation efficiency, spatial peak SAR, driving-point impedance and the far field.

A. Effective Radiation Efficiency

The effective radiation efficiency as a function of the distance (ρ) between the active dipole and sphere was computed for different reflector configurations. The lengths of the reflective element $2\boldsymbol{h}_r$ and the separation δ between the reflective and the active elements were varied. The results are shown in Figs. 11 and 12. As expected, the effective radiation efficiency increases with ρ for all configurations. The results were compared to a $\lambda/2$ dipole and they can be summarized as follows.

- The directive configuration shows a degradation in radiation performance because of the requirements for hand-held MTE applications. In this case, the active element is closer to the user's head $(\rho - \delta)$.
- The reflective configuration shows a very significant improvement in radiation performance at normal operating conditions, although the parasitic element is closer to the user's head $(\rho - \delta)$. As expected based on the free-space results, the radiation efficiency does hardly depend on the separation δ.
- When the antenna is far away from the user, the coupling of electromagnetic energy between the user and antenna is small. This is evident from the diminished radiation efficiency improvement.
- For $\boldsymbol{k} > 1.25$, the incremental radiation performance is small for larger $\boldsymbol{k}$ or δ.

For hand-held MTE, the separation distance ρ between the antenna and the user's face is between 15–30 mm. This trans-

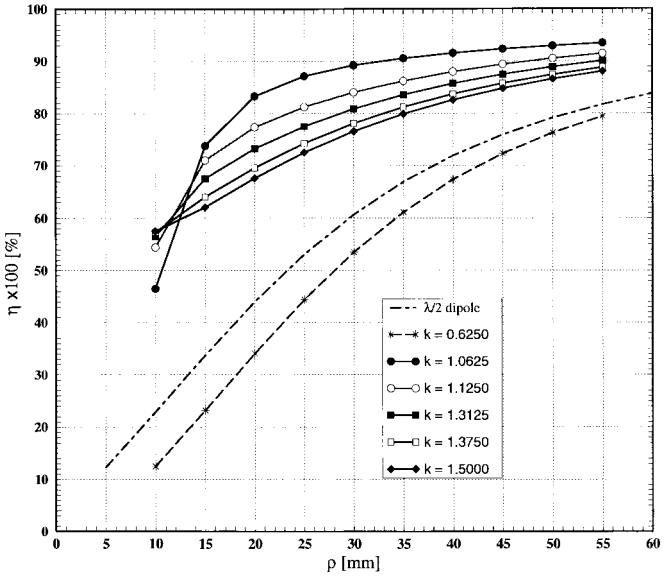

Fig. 11. Comparison of effective radiation efficiencies for reflectively coupled dipoles operating at 900 MHz with different heights ($\boldsymbol{k} > 1$) of the reflective element. The separation δ between the active dipole and the reflector was 0.015λ. The results were compared to the effective radiation efficiency of a $\lambda/2$ dipole and a $\lambda/2$ dipole coupled to a director with $\boldsymbol{k} = 0.625$ and $\delta = 0.015\lambda$.

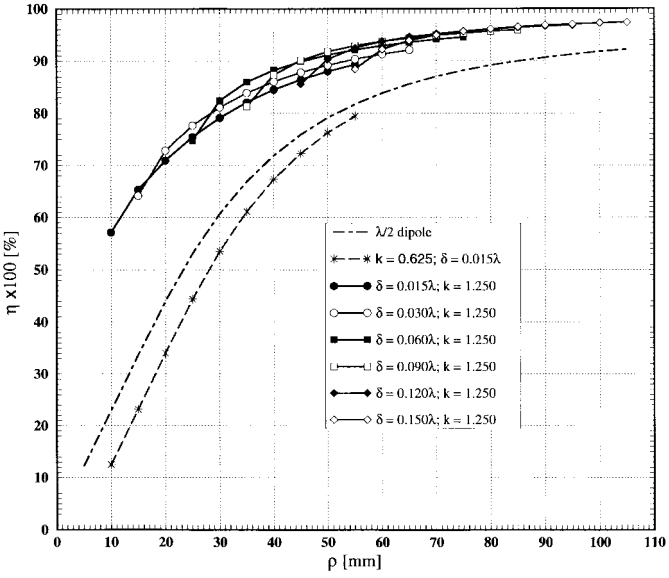

Fig. 12. Comparison of effective radiation efficiency at 900 MHz for reflectively coupled dipoles ($\boldsymbol{k} = 1.25$) having different separations δ between active and reflective elements. The results were compared to the effective radiation efficiency of the $\lambda/2$ dipole and a $\lambda/2$ dipole coupled to a director with $\boldsymbol{k} = 0.625$ and $\delta = 0.015\lambda$.

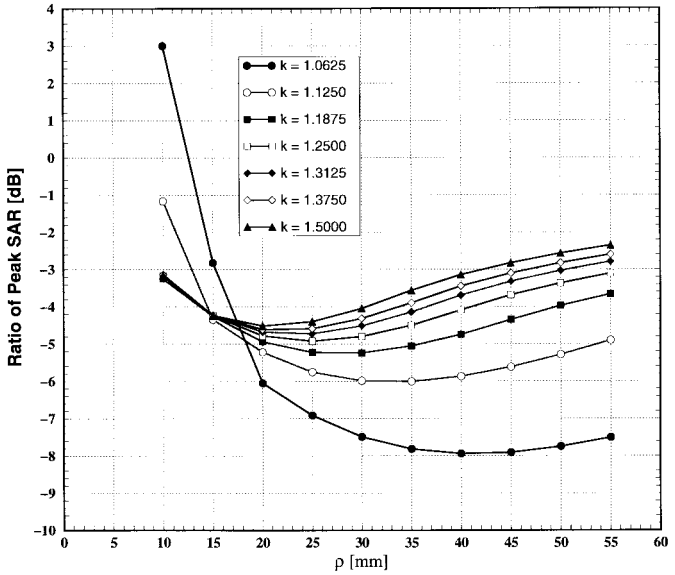

Fig. 13. Comparison between the ratio of maximum induced SAR for the reflectively coupled dipoles to the $\lambda/2$ dipole at 900 MHz as a function of the distance (ρ). The separation (δ) between the active dipole and the reflector was kept constant at 0.015λ, but the height of the reflective element was varied from $\boldsymbol{k} = 1.0625$ to $\boldsymbol{k} = 1.5$.

lates into an improvement in radiation efficiency of greater than 2 dB. As the trend for hand-held MTE is to develop smaller and lighter devices, the separation distance ρ is expected to reduce. Hence, effective radiation efficiency is expected to improve. In Fig. 12, the effective radiation efficiency increases with δ. However, the costs associated with implementing larger antennas into hand-held MTE devices are very high, especially in an era of miniaturization.

B. Spatial Peak SAR

In this investigation, the total power absorbed P_{abs} is reduced by the same ratio as the improvement in effective radiation efficiency because all antenna elements were simulated as perfect conductors (i.e., $P_{\text{diss}} = 0$). Since the reflectively coupled dipole not only reduces the maximum magnetic field strength but also widens the H-field distribution over a larger area, one may expect greater reduction of the peak SAR than for the sphere-averaged SAR or total power absorbed. In Fig. 13, the maximum locally induced SAR values are compared to a $\lambda/2$ dipole and to a directively coupled dipole as a function of the distance (ρ) between the active dipole and sphere. The improvement is significant for the entire range of distances (10–50 mm) and is better than -3 dB for the closest distances between the active dipole and the head except when $\boldsymbol{k}$ is very close to one, at which point the impedance is very low resulting in an increased magnetic field strength in the closest vicinity of the antenna. The greatly increased absorption for $\boldsymbol{k} = 1.0625$ confirms the prediction derived from the distribution of the incident H-field given in Fig. 8. However, because of the large gradient of the incident H-field, the peak is very local such that the overall radiation efficiency is still better than that of the dipole (see Fig. 11).

To verify these findings, the SAR distribution was compared with those of measurements using the setup described earlier

Fig. 14. The SAR distribution experimentally measured in the head phantom filled with brain simulating liquid ($\epsilon_r = 44$ and $\sigma = 1.0$℧/m). The reflectively coupled dipole with $\delta = 5$ mm and $\boldsymbol{k} = 1.25$ was positioned at the distance $\rho = 13$ mm. The darker shading denotes a higher SAR, which moves to a lighter (lower SAR) shading at the outer edges.

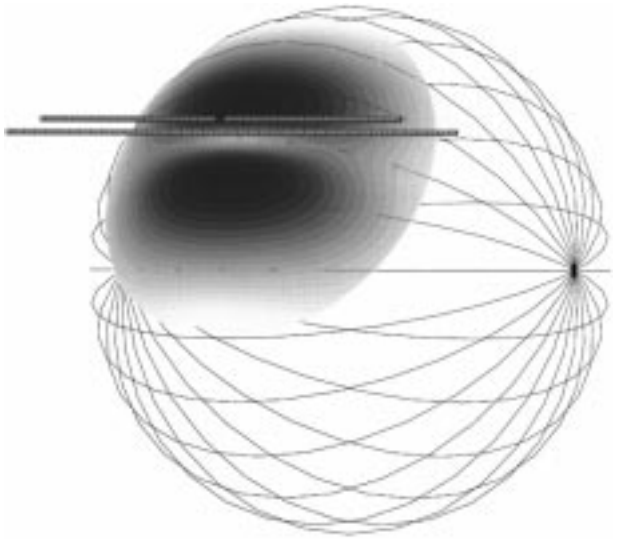

Fig. 15. The simulated SAR distribution in the spherical dielectric phantom ($\epsilon_r = 44$ and $\sigma = 1.0$℧/m). The reflectively coupled dipole of $\delta = 5$ mm and $\boldsymbol{k} = 1.25$ was positioned at the distance $\rho = 13$ mm. The darker shading denotes a higher SAR, which moves to a lighter (lower SAR) shading at the outer edges.

[2]. The experimental antenna ($\boldsymbol{k} = 1.25$ and $\delta = 0.015\lambda$) was positioned close to the phantom at a distance of 13 mm (reflector axis to the brain-simulating liquid). The SAR distribution was scanned in the tissue simulating liquid at the inner surface of the phantom shell. The simulated results were evaluated at the same distance from the surface. Since the electrical parameters of the brain simulating liquid were slightly different than those used in the previous computations, i.e., $\epsilon_r = 44$ and $\sigma = 1.0$℧/m, an additional simulation was performed with exactly the same parameters, except that a sphere phantom was used instead of a head phantom. The results are compared in Figs. 14 and 15. Comparing this induced field pattern with that of the incident H-field (Figs. 9 and 10), it does become very obvious that the fields are mainly induced by magnetic coupling as stated first in [1].

C. Driving Point Resistance

The third parameter to be optimized was the stability of the driving-point impedance. This is important in order to maintain the performance of the MTE independent of its position with respect to the head.

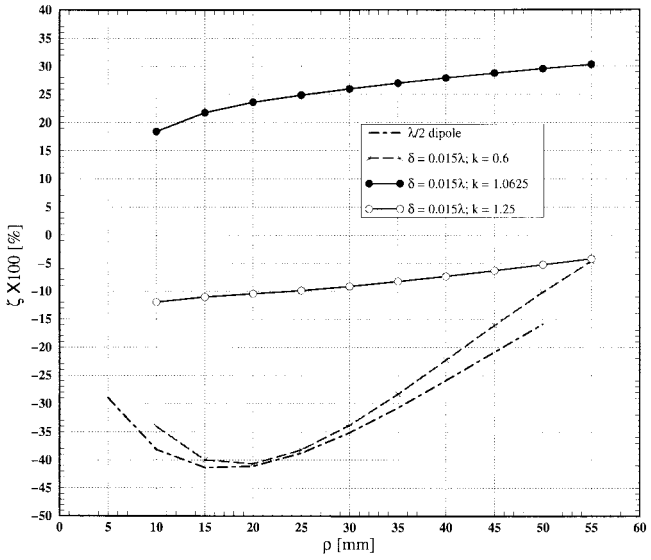

Fig. 16. Comparison of the change of input resistance at 900 MHz in free-space and in the presence of a scatterer for a $\lambda/2$ dipole, the same dipole coupled to a directive element of $\boldsymbol{k} = 0.625$ and the two cases with the reflective elements of $\boldsymbol{k} = 1.0625$ and $\boldsymbol{k} = 1.25$ whereby δ is 0.015λ in all cases.

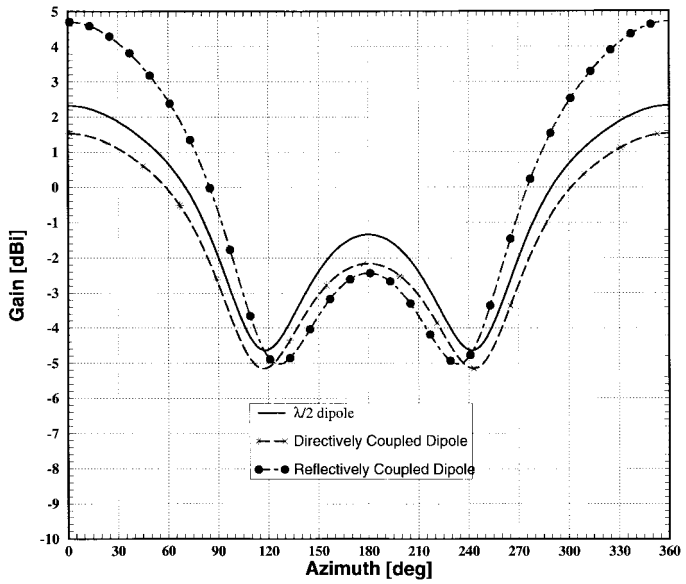

Fig. 17. Comparison of the far-field radiation plot in the xy plane (azimuth cut) between the $\lambda/2$ dipole, the directively coupled dipole, and the reflectively coupled dipole. The separation distance between the active element and the spherical phantom was 25 mm. The separation distance δ between the active element and the parasitic element was 0.015λ and the frequency was 900 MHz.

The sensitivity of the driving-point resistance on the distance from the sphere compared to the dipole is shown in Fig. 16. In conclusion:

- large variations of the driving-point resistance are observed for the $\lambda/2$ dipole and the directively-coupled $\lambda/2$ dipole;
- small and linear changes in the driving-point resistance were found for the reflectively coupled $\lambda/2$ dipole.

D. Far Field

The most instructive plots are those of the radiation pattern. Figs. 17 and 18 reveal that the improvement in gain between the reflectively coupled dipole and the $\lambda/2$ dipole is considerably better at the head than in free-space, whereas the losses on the rear of the head are minor. This improvement in gain is even more pronounced for smaller distances. At higher frequencies the relative reduction in gain in the shadow of the head will become less significant.

On the other hand, the performance of the directively coupled dipole deteriorates in all directions.

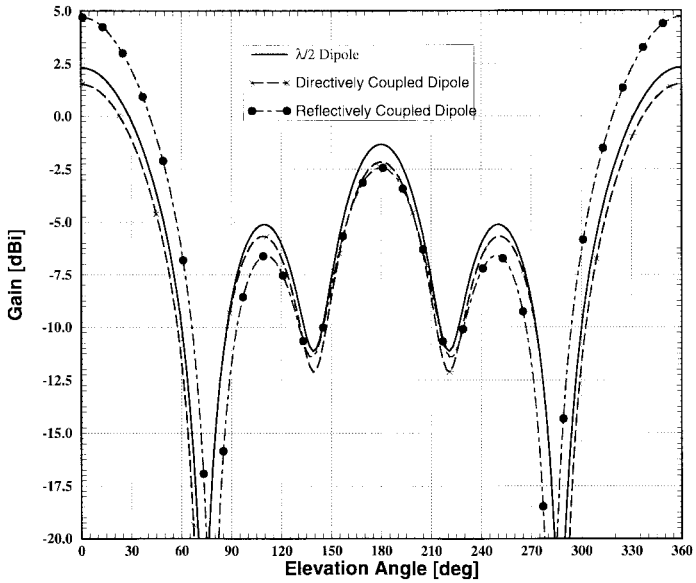

Fig. 18. Comparison of the far-field radiation plot in the xz plane (elevation cut) between the $\lambda/2$ dipole, the directively coupled dipole, and the reflectively coupled dipole. The separation distance between the active element and the spherical phantom was 25 mm. The separation distance δ between the active element and the parasitic element was 0.015λ and the frequency was 900 MHz.

VIII. Conclusions

This paper demonstrates that reduction of the magnetic field strength at the surface of the user's head is the key parameter to improve the efficiency of the transmitter. This has been demonstrated in the coarse of the study on the basis of a simple $\lambda/2$ dipole combined with a directive or reflective element. For example, a reflectively coupled dipole at 20-mm distance between antenna structure and head reduces the spatial peak SAR in the head by 4.7 dB and improves the effective radiation efficiency from 34 to 71% compared to the $\lambda/2$ dipole. On the other hand, other directive antenna structures reduced the antenna performance. Hence, directive antennas do not *per se* reduce the power loss in the head of the user. This reasoning also explains the relatively poor performance of helix antennas.

The reflectively coupled dipoles further reduced the dependence of the driving-point impedance upon the position of the antenna with respect to the scatterer. However, the disadvantages of this approach are a more complicated antenna structure, slightly larger antenna size compared to the $\lambda/2$ dipole, and an input impedance of below 10 Ω. In

addition, implementation of the reflectively coupled dipole for hand-held MTE applications requires great care. Incorrect orientation of the antenna during operation could cause severe radiation performance impairment and high electromagnetic (EM) energy absorption by the user. Nevertheless, reflectively coupled dipoles are an interesting alternative for mobile-phone antennas, especially in the 1–2-GHz band.

ACKNOWLEDGMENT

The authors would like to thank D. Zakharia for help during the experimental measurements.

REFERENCES

[1] N. Kuster and Q. Balzano, "Energy absorption mechanism by biological bodies in the near field of dipole antennas above 300 MHz," *IEEE Trans. Veh. Technol.*, vol. 41, pp. 17–23, Feb. 1992.
[2] V. Hombach, K. Meier, M. Burkhardt, E. Kühn, and N. Kuster, "The dependence of EM energy absorption upon human head modeling at 900 MHz," *Trans. Microwave Theory Tech.*, vol. 44, pp. 1865–1873, Oct. 1996.
[3] K. Meier, R. Kästle, V. Hombach, R. Tay, and N. Kuster, "The dependence of EM energy absorption upon human head modeling at 1800 MHz," *IEEE Trans. Microwave Theory Tech.*, vol. 45, pp. 2058–2062, Oct. 1997.
[4] R. Y.-S. Tay, "Contributions towards the optimization of hand-held mobile telecommunication equipment by computational electromagnetics," Ph.D. dissertation, Swiss Fed. Inst. Technol., Zurich, Switzerland, 1997.
[5] N. Kuster, Q. Balzano, and J. Lin, Eds., *Mobile Communications Safety*. London, U.K.: Chapman Hall, 1997, p. 273.
[6] L. Slesin, Ed., "Swiss Tests Show Wide Variation in Radiation Exposure from Cell Phones," *Microwave News*, vol. 17, no. 6, pp. 1–11, Dec. 1997.
[7] G. F. Pedersen and J. B. Andersen, "Integrated antennas for hand-held telephones with low absorption," in *Proc. 44th IEEE Veh. Technol. Conf.*, Stockholm, Sweden, June 1994, pp. 1537–1541.
[8] K. Noguchi, M. Ando, N.-h. Goto, M.-N. Hirose, T. Uno, and Y.-T. Kamimura, "Directional antennas for portable telephones," *IEICE Trans. Commun.*, vol. E79-B, no. 9, pp. 1234–1241, Sept. 1996.
[9] F. Schönborn, M. Burkhardt, and N. Kuster, "Differences in energy absorption between heads of adults and children in the near field of sources," *Health Phys.*, vol. 74, no. 2, pp. 160–168, Feb., 1997.
[10] R. Y.-S. Tay and N. Kuster, "Performance of the generalized multipole technique (GMT/MMP) in antenna design and optimization," *Appl. Computat. Electromagn. Soc. (ACES) J.*, vol. 9, no. 3, pp. 79–89, 1994.
[11] N. Kuster, "Multiple multipole method for simulating EM problems involving biological bodies," *IEEE Trans. Biomed. Eng.*, vol. 40, pp. 611–620, July 1993.
[12] C. Hafner and L. H. Bomholt, *The 3-D Electrodynamic Wave Simulator*. New York: Wiley, 1993.
[13] Q. Balzano, O. Garay, and F. R. Steel, "Heating of biological tissue in the induction field of VHF portable radio transmitters," *IEEE Trans. Veh. Technol.*, vol. VT-27, pp. 51–56, May 1978.
[14] G. Hartgrove, A. Kraszewski, and A. Surowiec, "Simulated biological materials for electromagnetic radiation absorption studies," *Bioelectromagn.*, vol. 8, no. 1, pp. 29–36, 1987.
[15] T. Schmid, O. Egger, and N. Kuster, "Automated E-field scanning system for dosimetric assessments," *IEEE Trans. Microwave Theory Tech.*, vol. 44, pp. 105–113, Jan. 1996.
[16] N. Kuster, R. Kästle, and T. Schmid, "Dosimetric evaluation of handheld mobile communications equipment with known precision," *IEICE Trans. Commun.*, vol. E80-B, no. 5, pp. 645–652, May 1997.

Roger Yew-Siow Tay (S'82–M'86) was born in Johor Baru, Malaysia, in 1958. He received the B.S. and the M.S. degrees in electrical engineering from the University of Massachusetts, Lowell, in 1983 and 1985, respectively, and the Ph.D. degree from the Swiss Federal Institute of Technology (ETH), Zurich, Switzerland, in 1997.

In 1987, he returned to the Far East and joined the Research and Development Department, Motorola Electronics Pte., Ltd., Singapore. In 1990 he was transferred to the Florida Electromagnetics Laboratory of Motorola Inc., Fort Lauderdale, FL. In 1993, he was invited as an Academic Guest to the ETH for eight months. He is currently Principal Staff Engineer with the Motorola Corporate Electromagnetics Research Laboratory, Fort Lauderdale. FL. He holds three patents and four pending patents and has contributed papers in many journals and conferences.

Dr. Tay is a member of the IEEE Antennas and Propagation and Electromagnetics Compatibility Societies. He is listed in *Marquis's Who's Who in Science and Engineering* and *Marquis's Who's Who in the World.*

Quirino Balzano (S'63–M'72–SM'83) received the Ph.D. degree in electronics from the University of Rome, Italy, in 1965.

From 1967 to 1974, he worked for the Missile System Division of Raytheon Company, Bedford, MD. Since 1974 he has been with the Communication Products Division of Motorola, Inc., Fort Lauderdale, FL, first as a Staff Engineer, then, in 1978, he was appointed Manager of the Antenna and Digital System Research Laboratory, and in 1987, he was appointed Vice President of the Technical Staff of Motorola and Manager of the communication systems research efforts. He was appointed Vice President and Director of the Portable Products Division in 1988, and, in 1990, Vice President of the Technical Staff of the Radio Products Group. In 1993 he was elected to the position of Corporate Vice President of Motorola. He holds 14 patents and has authored or coauthored over 50 papers and publications.

Dr. Balzano received the Best Paper of the Year Award from IEEE Vehicular Technology Group in 1978 and 1982. He is a Charter Member of the Bioelectromagnetic Society and a member of the IEEE Antennas and Propagation and Vehicular Societies.

Niels Kuster (M'93) was born in Olten, Switzerland, in June 1957. He received the Diploma and Ph.D. degrees in electrical engineering from the Swiss Federal Institute of Technology (ETH), Zurich, Switzerland.

In 1985, he joined the Electromagnetics Laboratory, ETH, where he was involved in the research and development of the generalized multipole technique (GMT) and the 3-D MMP code. In 1992 he was an invited Professor at Motorola Inc., Fort Lauderdale, FL for a trimester. He is currently a Professor at the Department of Electrical Engineering, ETH. His research interests include all aspects of numerical techniques in electrodynamics, near-field measurement techniques, antenna design, and biological effects of electromagnetic fields.

Dr. Kuster is a member of various scientific societies and official member of URSI Commission K.